

Contents lists available at ScienceDirect

# **Food Chemistry**

journal homepage: www.elsevier.com/locate/foodchem





# Investigating the synergistic effects of high-pressure homogenization and pH shifting on the formation of tryptophan-rich nanoparticles

Hongmin Dong <sup>a</sup>, Lixin Yang <sup>a</sup>, Younas Dadmohammadi <sup>a</sup>, Peilong Li <sup>a</sup>, Tiantian Lin <sup>a</sup>, Yanhong He <sup>a</sup>, Yufeng Zhou <sup>a</sup>, Jieying Li <sup>a</sup>, Gopinathan Meletharayil <sup>b</sup>, Rohit Kapoor <sup>b</sup>, Alireza Abbaspourrad <sup>a,\*</sup>

#### ARTICLE INFO

Keywords: α-lactalbumin Tryptophan Nanoparticles High-pressure homogenization pH-shifting

#### ABSTRACT

A combined treatment of high-pressure homogenization (HPH) and pH-shifting on the mixture of  $\alpha$ -lactalbumin ( $\alpha$ -LA) and tryptophan (Trp) was used to fabricate nanoparticles ( $\alpha$ -LA-Trp-NP). The optimal  $\alpha$ -LA-Trp ratio (5:1), HPH pressure (206.8 MPa), and recirculation time (40 min) was found to produce small  $\alpha$ -LA-Trp-NP (243.0  $\pm$  7.2 nm) with a narrow particle size distribution. Comparing the size and morphology of  $\alpha$ -LA-NPs with  $\alpha$ -LA-Trp-NPs indicated that the presence of Trp significantly affected the size and morphology of the NPs in the dry form. The stability of the  $\alpha$ -LA-Trp-NPs was improved by using the combination of HPH and pH-shifting. The  $\alpha$ -LA-Trp-NPs showed better freeze—thaw stability and retained the particle characteristics with heat treatment at 63 °C, 30 min after the freeze—thaw cycle.  $\alpha$ -LA-Trp-NPs were also observed to have remarkable stability against pH changes and thermal treatments at 63 °C, 30 min, and 90 °C, 2 min.

# 1. Introduction

L-Tryptophan (Trp) is an essential amino acid that plays a critical role in various biological processes, including growth, protein synthesis, and neurotransmitter synthesis. It is also involved in regulating mood, appetite, sleep, pain perception, and has demonstrated potential health benefits in disease management (Friedman, 2018). Therefore, Trp is considered an essential dietary component. The use of Trp as a food supplement, however, is limited due to its notably bitter taste, which is attributed to the indole ring, even at concentrations as low 4 mmol/L (Di Pizio & Nicoli, 2020). Therefore, effective strategies are needed to mask the bitterness of Trp to extend its use in functional food products. Trp can be found in high concentrations in eggs, milk, and meat. Specifically,  $\alpha$ -lactalbumin ( $\alpha$ -LA), a whey protein, contains a high level of Trp (5.8 w/w %) making it an ideal candidate for producing Trp-rich ingredients. Recent research in protein nanotechnology suggests that more promising outcomes can be achieved by manipulating protein structure, molecular self-assembly of nano- and macroscopic materials, or by developing new techniques to better dissolve protein molecules at the nanoscale (Wei et al., 2017).

Various techniques have been developed to reduce the bitter taste

associated with amino acids, including the addition of bitter tastereducing components and physical barriers (Ley, 2008). For example, incorporating Trp with β-cyclodextrin has been reported to reduce bitterness with β-cyclodextrin to Trp ratio of 5.6:1 (w/w) (Rudolph et al., 2018), however the Joint FAO/WHO Expert Committee on Food Additives (JECFA) recommends a maximal level of β-cyclodextrin of 5 mg kg<sup>-1</sup> per day in foods and adults need 4–6 mg kg<sup>-1</sup> of Trp daily. To achieve this level of Trp using  $\beta$ -cyclodextrin as an encapsulant, this approach may exceed the maximal recommended daily dose of  $\beta$ -cyclodextrin. As an alternative approach, complexation of bioactive compounds with protein biopolymers has gained attention as a means to mitigate their undesirable tastes. Incorporating Trp into protein biopolymers, especially whey proteins like  $\alpha$ -LA, shows promise as a potential solution to produce Trp-rich ingredients and reduce its undesirable taste (Zhang, Li, et al., 2020). However, there is currently limited information available regarding the complexation of Trp with whey protein. Recent studies have reported that high-pressure homogenization (HPH) can promote the interaction of proteins with other components, such as proteins and polysaccharides, to form larger aggregates (Zhu et al., 2021). High-pressure homogenization (HPH) involves the combined action of high shear force, cavitation, and

E-mail address: Alireza@cornell.edu (A. Abbaspourrad).

<sup>&</sup>lt;sup>a</sup> Department of Food Science, College of Agricultural and Life Sciences, Cornell University, Ithaca, NY 14853, USA

<sup>&</sup>lt;sup>b</sup> Dairy Management Inc., Rosemont, IL, USA

<sup>\*</sup> Corresponding author.

turbulence, to invoke structural changes in proteins (Ma et al., 2020). Meanwhile, HPH treatment has been shown to reduce particle size due to the pressure gradient force, making it a promising method for creating particles from molecules with small and uniform particle size distributions (Zhu et al., 2021). The dual effects of HPH, the facilitation of the interaction of proteins with other components and the reduction of particle size, makes it a versatile method for creating new nanoparticles. However, to the best of our knowledge, the effect of the HPH treatment on Trp and  $\alpha\text{-LA-Trp}$  complexes has not been investigated.

Additionally, pH-shifting has been shown to substantially improve protein solubility, hydrophobicity, disulfide bond aggregation, as well as emulsifying and interfacial properties of proteins (Jiang et al., 2009, 2018; Tang, 2020). In this approach, proteins are treated at extreme pH conditions followed by neutralization. The protein structures are expected to unfold or dissociate into polypeptide molecules at extreme pH levels such as pH 11, and the unfolded protein molecules refold or self-assemble into soluble aggregates when the pH level is shifted back to neutral conditions. At high pH levels, such as pH 11, the protein is less tightly folded providing open sites for the incorporation of Trp. Then HPH can be used to force the protein to incorporate Trp molecules. When the pH is shifted once again to lower pH after HPH the protein to folds and compresses around the Trp molecules producing nanoparticles (NP) enriched in tryptophan. To date, there is limited information about the combined effect of pH shifting with HPH.

Here, we report the preparation of  $\alpha\text{-LA-Trp-NPs}$  by HPH treatment of a mixture of  $\alpha\text{-LA}$  and Trp at pH 11, followed by neutralization to pH 7. The combined effect on NP formation of HPH with pH shifting was investigated. The formation conditions for the NPs were optimized based on particle size, particle size distribution, and polydispersity index (PDI). The mechanism of  $\alpha\text{-LA-Trp-NP}$  formation was investigated using Trp fluorescence spectra. Finally, the synergistic effects of HPH and pH shifting on NP stability, such as pH-, thermal-, freeze–thaw-, and freeze–thaw-thermal stability, were evaluated. The outcomes of the present work provide a new approach to forming Trp-rich nanoparticles with improved stability.

#### 2. Materials and methods

### 2.1. Materials

Bovine milk  $\alpha$ -lactalbumin ( $\alpha$ -LA) powder was provided by Agropur, USA (batch number, JE 0001-21-414, 92.5% purity). Tryptophan (Trp) was purchased from Sigma (Reagent grade  $\geq$ 98%, St. Louis, MO, USA). Hydrochloric acid (HCl, ACS grade) and sodium hydroxide (NaOH, 98%) were purchased from Fisher Scientific (Hampton, NH, USA). All water used was Milli-Q water. Milli-Q water (18.2 M $\Omega$ /cm) was produced using a Millipore water purification system (Millipore Sigma, Burlington, MA, USA).

#### 2.2. Preparation of $\alpha$ -LA-Trp-NPs

 $\alpha\text{-LA-Trp-NPs}$  were prepared using a high-pressure homogenization-pH shifting technique. Briefly, the mixtures of  $\alpha\text{-LA}$  and Trp were fully dissolved in Milli-Q water by adjusting pH to 11 using 1 N NaOH solution to unfold the protein. The mixture was then passed through a high-pressure homogenizer (HPH) (Nano DeBee, Bee International, inc. USA) and recirculated. After recirculation, the pH of the solutions was adjusted to both neutral (pH 11  $\rightarrow$  7), and acidic (pH 11  $\rightarrow$  3), conditions using 1 N HCl to refold the protein and effectively encapsulate the Trp within it. For comparison, control samples,  $\alpha\text{-LA-NPs}$  without Trp and Trp-NPs without  $\alpha\text{-LA}$ , were prepared using similar procedures.

# 2.3. Optimization of $\alpha$ -LA-Trp-NPs

Optimization of the  $\alpha$ -LA to Trp ratios and the HPH pressure and recirculation times were carried out to formulate  $\alpha$ -LA-Trp-NPs with

optimal physicochemical characteristics based on the particle size, particle size distribution, polydispersity index (PDI), and tryptophan fluorescence intensity (TFI). After conducting a series of preliminary studies (data not shown), a total combined concentration of 100 mg  $\mbox{mL}^{-1}$  for  $\alpha\mbox{-LA}$  and Trp was selected. This concentration was found to result in a uniform particle size distribution, as confirmed by Dynamic Light Scattering (DLS) at the highest concentration tested. The optimal PDI value was <0.3. Different  $\alpha$ -LA to Trp w/w % ratios (20:1, 15:1, 10:1, 5:1, 4:1, and 3:1) were tested while keeping the HPH pressure (206.8 MPa) and recirculation time (30 min) constant.  $\alpha$ -LA-Trp-NPs were prepared at different HPH pressures (6.9, 34.5, 68.9, 137.9, 206.8, and 275.8 MPa (1,000-40,000PSI)) while mass ratio and recirculation time (30 min) were kept constant. Finally, the effect of recirculation time (5, 10, 20, 30, 40, and 50 min) was explored by keeping the HPH pressure (206.8 MPa) and the mass ratio constant. The effect of pH shifting (pH 11, from pH 11 to 7 and from pH 11 to 3) on the α-LA-Trp-NPs formation were investigated only at the optimized conditions. For comparison, control samples, α-LA-NPs without Trp and Trp-NPs without  $\alpha$ -LA, were prepared at the optimized conditions.

# 2.4. Measurements of particle size, particle size distribution, and polydispersity index

The particle size, particle size distribution, and PDI values of the NPs were determined by dynamic light scattering (DLS) using a Zetasizer (Nano S, Malvern Instruments, Worcestershire, UK). The measurements were performed at a scattering angle of  $173^{\circ}$ , at  $25~^{\circ}$ C;  $15~^{\circ}$ C in such that were done for each measurement. Particle size distribution can also be reflected by PDI values ranging between 0 and 1; a small PDI value indicates a narrow size distribution. In most cases, a monodispersed particle system would have a PDI <0.3. All measurements were carried out in triplicate.

# 2.5. Turbidity measurements

The turbidity of the  $\alpha$ -LA-Trp mixtures was measured using a UV–vis spectrophotometer (UV-2600, SHIMADZU Co., Japan). Sample solutions were analyzed at room temperature and the transmittance was measured at 600 nm. Milli-Q water was used as the blank (100% transmittance). The turbidity (T) was calculated as follows (Eq. (1)):

$$T = -\ln\frac{I}{I_0} \tag{1}$$

where I is the transmittance intensity of the sample solution and  $I_0$  is the transmittance intensity of the blank.

#### 2.6. Tryptophan fluorescence spectra analysis

The tryptophan fluorescence spectra were collected using a spectrofluorometer (SHIMADZU, RF-6000, Japan) according to a previous method with some modifications (Zhu et al., 2021). Briefly, the fluorescence excitation wavelength was set at 295 nm, and the emission was recorded in a range between 310 and 500 nm. Data were collected at a step resolution of 0.5 nm. The change in fluorescence intensity of the protein and its combination with tryptophan was monitored during nanoparticle formation.

# 2.7. Scanning electron microscopy (SEM)

The morphology of the samples was observed using an SEM (Zeiss Gemini 500, Jena, Germany). Samples were directly mounted on an SEM plate with a carbon conductive tab before coating, while liquid samples that had not been freeze-dried were diluted with PBS (10 mM, pH 7) to a concentration of 1 mg mL $^{-1}$  and dripped onto an SEM plate with carbon conductive tab and then vacuum dried. All samples were coated with

carbon using a sputter coater (Denton Desk V, New Jersey, USA) and were then scanned by SEM with 1 keV and imaged by a high-efficiency secondary electron detector with a 20.0  $\mu$ m aperture.

#### 2.8. Thermal stability

The thermal stability of the prepared samples was investigated at two different temperatures. Freshly prepared samples were incubated at 63  $^{\circ}\text{C}$  for 30 min (pasteurization) and separate samples were incubated at 90  $^{\circ}\text{C}$  for 2 min (flash pasteurization) (Roca et al., 2013). The samples were then cooled to 25  $^{\circ}\text{C}$  and the appearance, turbidity, particle size, particle size distribution, and PDI were measured.

#### 2.9. Freeze-thaw and freeze-thaw-thermal stability

The freeze–thaw and freeze–thaw-thermal stability of the prepared samples were investigated and compared. Freshly prepared samples were stored in a freezer at  $-20\,^{\circ}\text{C}$  overnight and then transferred to a water bath with a temperature set at 25  $^{\circ}\text{C}$  for 2 h until completely thawed (Zhu et al., 2017). The appearance, turbidity, particle size, and particle size distribution were recorded after the freeze–thaw cycle. Additionally, samples that were freeze-thawed were then heated at 63  $^{\circ}\text{C}$  for 30 min to investigate the impact of freezing and thawing on thermal stability.

### 2.10. Statistical analysis

All experiments were performed in triplicate. Results are presented as mean  $\pm$  SD (standard deviation). The significance between means was established using one-way ANOVA (OriginPro 9.0.0, OriginLab Northampton, MA, USA).

JMP Pro 16.0.0 software (SAS Institute Inc., Cary, NC, USA) was used to optimize the experimental design and to analyze the data. To perform sensitivity analysis of processing parameters, we adopted the Design of Experiment (DOE) approach. For this study, a Full Factorial Design  $(3^K)$  strategy was selected, and two variables (K=2) were analyzed: HPH pressure  $(X_1,$  in MPa) and recirculation time  $(X_2,$  in min). The investigated responses were particle size  $(Y_1)$  and TFI  $(Y_2)$  at pH 11, particle size  $(Y_3)$ , and TFI  $(Y_4)$  at pH 7.

# 3. Results and discussions

HPH and pH shifting were used to form nanoparticles containing α-LA and Trp. At high pH the protein unfolded providing open sites and areas for the incorporation of Trp. HPH mixed the protein and the Trp molecules together and formed nanoparticles, α-LA-Trp-NPs. The pH of the α-LA-Trp-NPs solutions was then neutralized (pH 7), and the proteins folded around the Trp, making the NP size smaller and reduced the PDI and as a result the α-LA-Trp-NPs after HPH and pH shifting showed higher thermal and freeze-thaw thermal stability. We present the results of the formation of the NPs and their physicochemical properties under different formation conditions and storage treatments. We had two main objectives: first, to create \alpha-LA-Trp-NPs with a high concentration of incorporated Trp to α-LA exhibiting strong Trp fluorescence; and second, to achieve small particles with uniform size distributions that have excellent thermal stability. α-LA-Trp-NPs with these characteristics could have great potential for applications within the dairy industry, specifically in milk-based beverages.

# 3.1. The effect of HPH on the formation of $\alpha$ -LA-Trp-NPs

To understand the effect of HPH pressure on the physicochemical properties of the resulting  $\alpha\text{-LA-Trp-NPs},$  we maintained a constant  $\alpha\text{-LA}$  to Trp ratio of 20:1 (w/w) at pH 11. The samples were then subjected to recirculation for 30 min, while varying the HPH pressures. The particle size distribution, mean particle size and PDI values of  $\alpha\text{-LA-Trp-NPs}$ 

were measured using DLS (Fig. 1). The particle size and PDI value of α-LA-Trp-NPs increases as the pressure increases from 6.9 to 34.5 MPa, and then decreases when the pressure was above 34.5 MPa (Fig. 1A). Generally, the particle size of α-LA-Trp-NPs formed under high pressure (>68.9 MPa) decreased and became more uniform (PDI < 0.3) than those formed under low pressure.  $\alpha$ -LA-Trp-NPs obtained under pressure >206.8 MPa showed a narrow particle size distribution with a mean particle size  $\sim$ 290 nm. This is possibly due to the higher shear force, cavitation, and turbulence under high pressure, which facilitates protein aggregation and the formation of colloidal particles derived from protein aggregation under more homogeneous reaction conditions which is consistent with previous studies (Zhang, Wang, et al., 2022; Zhu et al., 2021). The mean particle size of  $\alpha$ -LA-Trp-NPs formed decreased from 436 to 271 nm with increasing HPH pressure from 68.9 to 275.8 MPa. PDI decreased from 0.29 at 68.9 MPa to 0.15 at 206.8 MPa, but then slightly increased to 0.19 at 275.8 MPa. We attribute this phenomenon, where particles become polydisperse with increasing HPH pressure, to greater intermolecular interactions available at certain levels of pressures which break down at higher pressure.

Our goal was to incorporate as much Trp into the NPs as possible while forming the smallest and most uniform NPs, therefore, the effect of  $\alpha\text{-LA}$  to Trp ratios (20:1, 15:1, 10:1, 5:1, 4:1, and 3:1 w/w), on the particle size of  $\alpha\text{-LA-Trp-NPs}$  was performed under a set HPH pressure of 206.8 MPa and a recirculation time of 30 min. Between the range of 20:1 and 5:1  $\alpha\text{-LA}$  to Trp ratios, we observed no significant changes in the particle size and PDI values, these NPs showed a narrow particle size distribution with a mean particle size  $\sim\!290$  nm (Fig. 1B). When the Trp content was increased to a  $\alpha\text{-LA}$  to Trp ratio of 4:1 and 3:1, the particle size decreased significantly and were not uniform (PDI > 0.3). Therefore, the  $\alpha\text{-LA/Trp}$  ratio of 5:1 was selected for further study as it provided the highest Trp ration and the most uniform particle size and PDI.

The recirculation time was the final factor investigated. We used an HPH pressure of 206.8 MPa and an  $\alpha\text{-LA/Trp}$  ratio of 5:1. As a control group, we included samples that did not undergo HPH treatment (NOHPH). By varying the recirculation time under these conditions, we aimed to examine its influence on the physicochemical properties of the  $\alpha$ -LA-Trp-NPs. The particle size and PDI values of  $\alpha$ -LA-Trp-NPs decreased with increasing recirculation time from 5 to 30 min, and then reached a plateau of mean particle size of  $\sim\!290$  nm from 30 min (Fig. 1C). Comparing the particle size of  $\alpha$ -LA-Trp mixture ( $\alpha$ -LA/Trp of 5:1, w/w) that was not treated with HPH (0 min) at pH 11, the particle size of  $\alpha$ -LA-Trp-NPs increased from 7 nm with PDI value of 0.37 to 332 nm with PDI value of 0.26 after 5 min HPH. This result indicated that HPH induced the aggregation of α-LA and Trp molecules forming large particles within 5 min under HPH at a pressure of 206.8 MPa. The influence of HPH pressure and recirculation time on the particle size of protein and polysaccharide complex nanoparticles, where high HPH pressure or long treatment time induces the formation of large aggregates of protein and polysaccharide due to hydrophobic interactions, has been reported (Zhu et al., 2021). Similar results were found in other studies on protein aggregates as influenced by HPH pressure and time (Saricaoglu et al., 2017; Wu et al., 2019).

### 3.2. Detection of aggregation induced by HPH via tryptophan fluorescence

The aggregation mechanism of the  $\alpha$ -LA and Trp mixtures was studied by monitoring the change in both the turbidity and the Trp fluorescence change during HPH. Trp fluorescence is linked to aggregation; increasing aggregation of Trp molecules causes the Trp chromophore to increase, or turn on; while at lower aggregation, the Trp turns off or exhibits lower fluorescence (Liu, Wolstenholme, et al., 2018). The intensity increase caused by aggregation of Trp molecules induced by HPH was investigated and compared at a fixed Trp content of 5:1  $\alpha$ -LA to Trp. Fluorescence intensity of samples subjected to various HPH pressures, specifically 68.9, 137.9, 206.8, and 275.5 MPa, with differing recirculation times of 20, 30, and 40 min was investigated

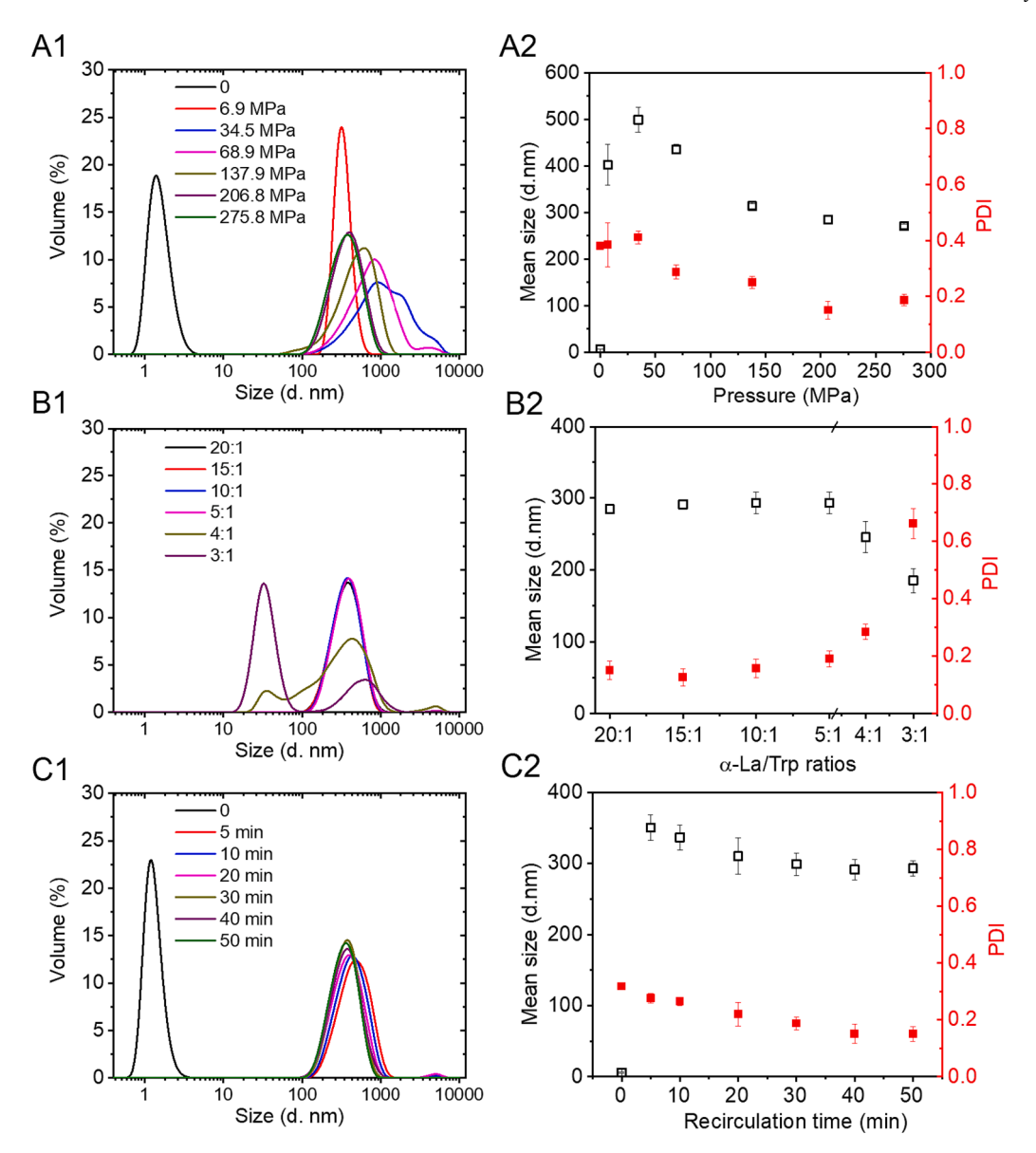


**Fig. 1.** Particle size distribution, mean sizes (open square) and PDI (polydisperse index, solid square) of  $\alpha$ -LA-Trp-NPs prepared at different conditions. A) the effect of pressure (with  $\alpha$ -LA/Trp ratio of 20:1 at pH 11, recirculation 30 min); B) the effect of  $\alpha$ -LA/Trp ratios (under HPH pressure of 206.8 MPa for 30 min); C) the effect of recirculation time (with  $\alpha$ -LA/Trp ratio of 5:1 at pH11, under HPH pressure of 206.8 MPa.

(Fig. 2A). Initially, the α-LA-Trp mixture at pH 11 without HPH showed weak fluorescence emission due to the pH dependent unfolding of the protein with free tryptophan molecules which indicated that without HPH very little of the protein and Trp were aggregated (Fig. 2A). However, after 20 min of HPH treatment for all samples treated at different pressure range of 68.9-275.8 MPa, a significant increase in fluorescence intensity was observed, exhibiting ~35-50-fold increase (Fig. 2A1); however little change was found at pressures between 68.9 and 206.8 MPa while a decrease was observed at 275.8 MPa. Furthermore, this increase in fluorescence intensity continued as the HPH recirculation times are extended to 30 and 40 min across all samples treated at different pressure ranges of 68.9-275.8 MPa (Fig. 2A2-3). Notably, variations in fluorescence intensity are observable within the pressure range of 68.9 to 275.8 MPa and the increase becomes more pronounced with longer recirculation times. With recirculation time of 40 min, the peak fluorescence intensity of the samples followed the order 137.9 MPa > 68.9 MPa > 206.8 MPa > 275.8 MPa. Considering the smaller and more uniform particle formed under higher pressure, we further optimized the HPH pressure (137.9, 206.8, and 275.8 MPa) and

recirculation time (20, 30, and 40 min) as suggested by Full Factorial Design (FFD) using the Design of Experiments function of the JMP 16.0 software. Based on the goal of minimize particle size with uniform particle size distribution (minimize PDI) and maximization of the Trp fluorescence intensity (Fig. S1 and Table S1), we selected an optimized HPH pressure of 206.8 MPa (30,000 PSI) and a recirculation time of 40 min. These conditions had the highest desirability value of 0.81 in the FFD (Fig. S1B).

The aggregation of the  $\alpha$ -LA and Trp was then further investigated at an HPH pressure of 206.8 MPa at recirculation time from 0 to 50 min and compared with turbidity for each sample (Fig. 2B). Consistently, the Trp fluorescence intensity increased with increasing time. However, after 50 min, the fluorescence intensity no longer showed an increase (Fig. 2B1). A positive correlation between the two factors was found (Fig. 2B2), confirming that HPH does induce aggregation between Trp and  $\alpha$ -LA. These results are consistent with the visual differences observed in the turbidity of colloidal dispersions formed after HPH under varying recirculation times (Fig. 2B3). These observations were in agreement with previous studies which reported that fluorescent

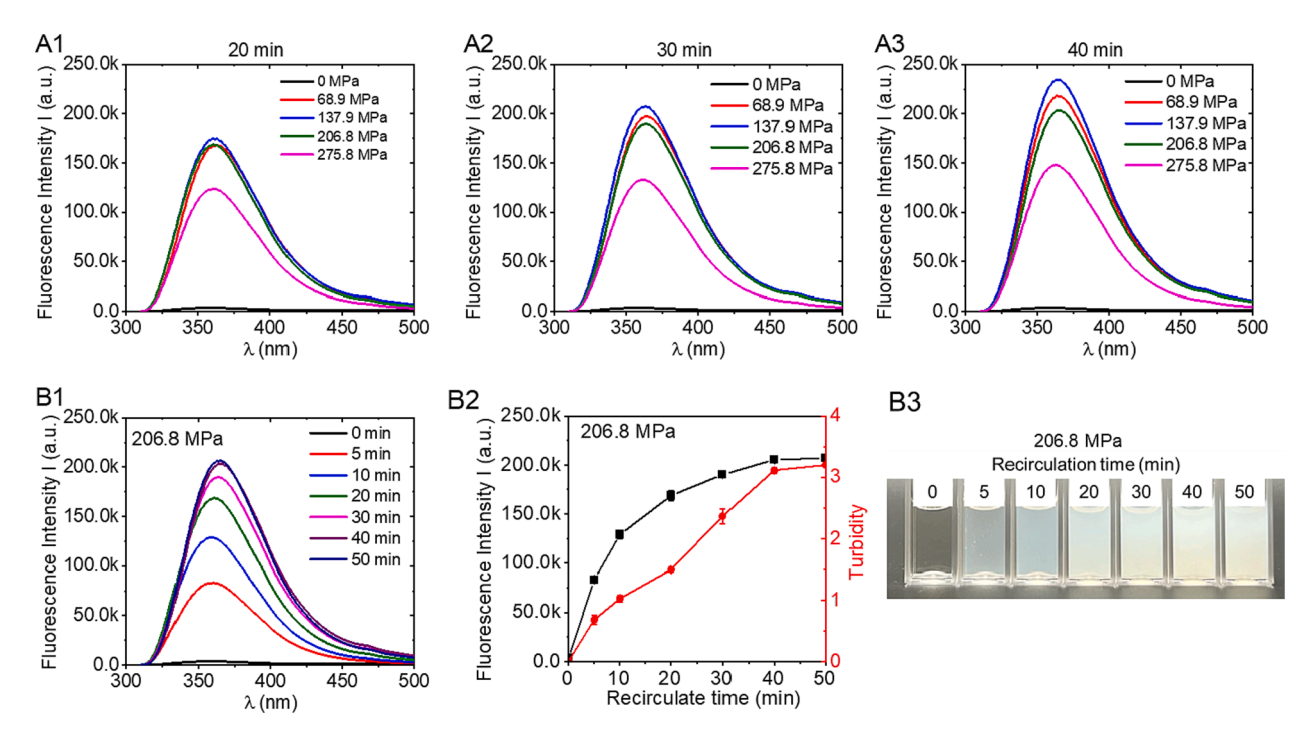


Fig. 2. Detection of protein aggregates. A) HPH-induced self-assembly of  $\alpha$ -LA and Trp increases the fluorescence intensity of Trp under different HPH conditions. B) Fluorescence and turbidity changes during extended treatment with HPH at 206.8 MPa and photographs of  $\alpha$ -LA-Trp-NPs aqueous suspension obtained under different recirculation time.

chromophores detect both unfolded soluble proteins via a turn off mechanism characterized by weak fluorescence, and insoluble aggregates or nanoparticles via the turn on mechanism characterized by strong fluorescence (Stănciuc et al., 2012; Toprakcioglu et al., 2019; Yu et al., 2021).

The increased fluorescence intensity and turbidity of the colloidal dispersion after HPH treatment indicate the formation of larger aggregates containing high amounts of Trp and confirming that HPH promotes the association of Trp with  $\alpha\text{-LA}$ . We also observed that the maximum emission wavelength of  $\alpha\text{-LA-Trp-NPs}$  was significantly redshifted with increasing HPH treatment time. This phenomenon can be explained by the distinctive emission wavelengths of  $\alpha\text{-LA}$  and Trp in the nanoparticles. When Trp is present within  $\alpha\text{-LA}$  (intrinsic Trp), it exhibits a maximum emission wavelength of approximately 350 nm at pH 11. However, Trp molecules, when aggregated independently or with a protein, display a higher maximum emission wavelength of around 360 nm. Consequently, during the formation of nanoparticles under different HPH treatment times, the maximum emission wavelength undergoes a red-shift due to the incorporation of a higher number of Trp molecules within the protein nanoparticles/aggregates.

The decrease in fluorescence intensity of  $\alpha$ -LA-Trp-NPs with increasing HPH pressure can be attributed to the changes in the particle size of the aggregates induced by HPH treatment. Notably, higher HPH pressure led to the formation of smaller particles, resulting in a larger surface area where more Trp molecules were exposed. Consequently, this increased surface presentation of Trp led to decreased fluorescence intensity due the solvent quenching (Stănciuc et al., 2012; Toptygin et al., 2002; Vivian & Callis, 2001). Overall, the choice of HPH conditions should be carefully considered based on the specific applications of α-LA-Trp-NPs. Different applications may require different characteristics, and a balance between particle size and fluorescence intensity needs to be achieved. For instance, in the beverage industry, small and uniform particle size distribution is crucial to ensure consistent product quality and stability. In making smaller particles, we also need to maximize the fluorescence because the higher it is, the greater aggregation between a-LA and Trp and the better the protein may mask the

bitter taste of Trp. Our main goal is to produce Trp-rich particles with a small and uniform particle size distribution while maximizing fluorescence intensity. To achieve this, we have selected an HPH pressure of 206.8 MPa and a recirculation time of 40 min, which balanced particle size, PDI, and fluorescence intensity as shown in Table S1 and Fig. S1. To evaluate the interactions between  $\alpha$ -LA and Trp in the  $\alpha$ -LA-Trp-NPs we will prepare  $\alpha$ -LA-NPs and Trp-NPs for comparison under our optimized HPH conditions during pH-shifting and thermal treatments.

# 3.3. The effect of pH shifting on the $\alpha$ -LA-Trp-NPs

pH shifting from pH 11 to neutral pH was conducted with the aim of enhancing the thermal stability of nanoparticles. The process involved the refolding and reassociation of the protein within the nanoparticles, which was expected to improve thermal stability (Jiang et al., 2009, 2018; Tang, 2020). Furthermore, to expand the potential applications of the  $\alpha$ -LA-Trp-NPs in the food industry, the colloidal dispersion induced by HPH at pH 11 was subjected to pH shifting to achieve both neutral (from pH 11 to 7) and highly acidic (from pH 11 to 3) conditions.

The colloidal stability was studied by visual observation, turbidity, particle size, and fluorescence measurements (Fig. 3 and Table S2). During pH shifting from 11 to 7 or from pH 11 to 3, the visual characteristics of the colloidal dispersion of α-LA-Trp-NPs remained unchanged. There were no noticeable changes in the appearance or in the measured turbidity of the colloidal dispersion, indicating that the nanoparticles maintained their stability throughout the pH adjustments (Fig. 3A and Table S2). This is consistent with the particle size and fluorescence results (Fig. 3C and D), where  $\alpha$ -LA-Trp-NPs showed larger size particles with strong fluorescence compared to those that were not treated with HPH (NOHPH) (Fig. 3B and D). This result is consistent with a previous study on NPs stabilized by whey protein that were shown to be stable at neutral and highly acidic conditions (Mehrad et al., 2018). The particle size of  $\alpha$ -LA-Trp-NPs was 290 nm and 240 nm with narrow particle size distribution (PDI < 0.2) at pH 11 and 7, respectively. This result indicated the particles formed at pH 11 remain uniform when pH shifted to neutral conditions. The slight decrease in

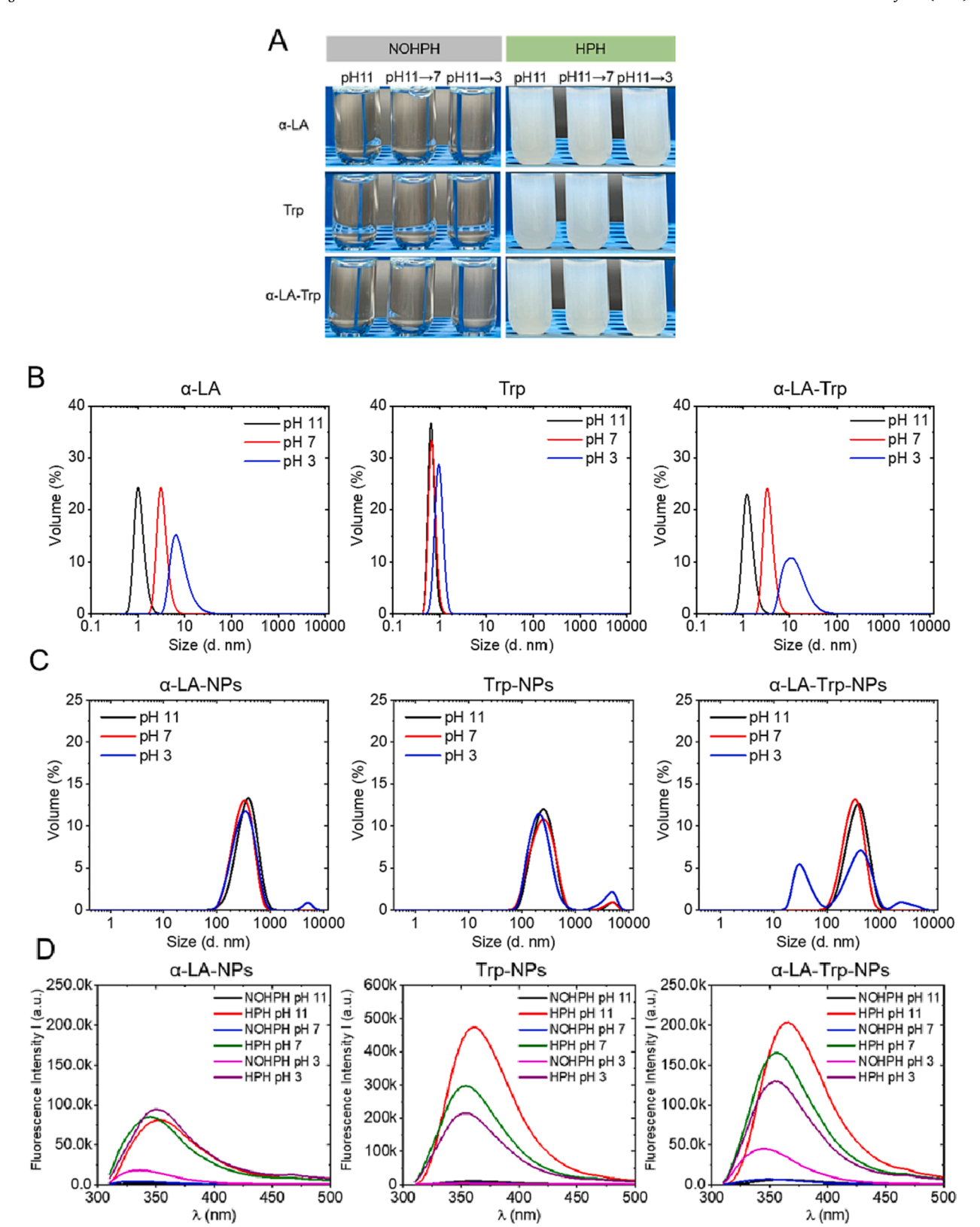


Fig. 3. A) Images of NOHPH and HPH samples from  $\alpha$ -LA, Trp, and  $\alpha$ -LA-Trp mixture; B) Particle size distributions of  $\alpha$ -LA, Trp, and  $\alpha$ -LA-Trp mixture without HPH (NOHPH); C) Particle size distributions of  $\alpha$ -LA-NPs, Trp-NPs, and  $\alpha$ -LA-Trp-NPs; D) Fluorescence spectroscopy of the  $\alpha$ -LA, Trp, and  $\alpha$ -LA-Trp mixture with and without HPH treatment. Excitation wavelength was 295 nm. HPH (High-pressure homogenization) samples were NPs formed at  $\alpha$ -LA/Trp ratio of 5:1, 206.8 MPa, 40 min at pH 11 and those with pH shifting from 11 to 7 and 11 to 3. NOHPH samples were prepared under same condition without HPH treatment.

particle size with pH shifting we attribute to the molecular associations, such as hydrophobic interaction, electrostatic interaction, hydrogen bonding, which may be enhanced during the pH shifting, resulting in a more highly packed structure where protein molecules exhibit a higher degree of folding in the nanoparticles at pH 7 (Jiang et al., 2009).

At lower pH the solution environment impacted the particle size of  $\alpha\text{-LA-Trp-NPs}$ . Where the PDI value of the  $\alpha\text{-LA-Trp-NPs}$  at pH 3 was significantly increased, and a peak for small-size particles ranging from 20 to 100 nm was observed. The presence of smaller particles implies that the particles were partially broken-down during pH shifting from 11 to 3. Conversely, the swelling behavor of the protein at pH 3 resulted in an increase in the particle size and thus the peak was shifted to a large-size particle range for NOHPH and a peak for larger-size particles was also observed for HPH samples (Fig. 4B and C).

The particle size change of the  $\alpha$ -LA-Trp-NPs at different pH shifting was consistent with their changes in fluorescence intensity (Fig. 3D), where larger size particles showing stronger fluorescence intensity. The red shift of fluorescence emission may be due to the change of the environment around Trp molecules, including pH changes, swelling, contracting, or breaking down of the particles (Stănciuc et al., 2012; Toptygin et al., 2002; Vivian & Callis, 2001).

NPs were also formed from  $\alpha$ -LA and Trp individually under the same conditions. The particle size of the  $\alpha$ -LA-NPs were similar to that of  $\alpha$ -LA-Trp-NPs, while Trp-NPs showed smaller particle size  $\sim\!210$  nm at all three pH levels. This is mainly due to the self-assembly behavior of both  $\alpha$ -LA and Trp (Bhangu et al., 2020; De et al., 2021; Liu, Fan, et al., 2018). Compared to NPs formed from  $\alpha$ -LA or Trp alone which were largely unchanged, the size distribution of NPs formed from their mixture

( $\alpha$ -LA-Trp-NPs) fluctuated during pH shifting from 11 to 3. These results indicated the interaction induced by the aggregation of  $\alpha$ -LA or Trp alone, showed better stability during pH shifting from 11 to 3 than those of their mixture. When the  $\alpha$ -LA-Trp-NPs where pH shifted from 11 to 3, a slight release of small particles from the large particles was observed. Overall, the  $\alpha$ -LA-Trp-NPs formed by HPH were found maintained their particle/aggregates status in a wide pH range, making them useful for different food matrices and nutrient processing conditions.

In summary,  $\alpha$ -LA, Trp, and a mixture of  $\alpha$ -LA and Trp were suspended in water and dissolved by adjusting the pH to 11. At high pH the intermolecular attractions of  $\alpha$ -LA, such as disulfide bonds, hydrophobic interactions, and electrostatic interactions, are reduced and its solubility increases as the protein unfolds (Jiang et al., 2009, 2018; Tang, 2020). By decreasing the inter- and intramolecular attractions in  $\alpha$ -LA, the possibility for the formation of new intermolecular interactions, bonds, and structures between the protein and Trp increases. Once the solutions were dissolved, we evaluated the effect of pH shifting with and without HPH. Shifting pH from pH 11 to a lower pH without HPH did not change the appearance of the solutions of  $\alpha$ -LA, Trp, and the mixture of  $\alpha$ -LA and Trp; they all remained clear solutions.

The particle sizes of  $\alpha$ -LA, and the  $\alpha$ -LA and Trp mixture, without HPH (NOHPH) slightly increased during pH shifting. This increase is related to the formation of soluble aggregates with a size range of 2–10 nm (Fig. 3B). The presence of Trp in the mixture with  $\alpha$ -LA slightly increased the particle size of the protein at all pH levels (11, 7 and 3) indicating the complex formation between  $\alpha$ -LA-Trp.

When HPH was applied to solutions of  $\alpha$ -LA, Trp, and  $\alpha$ -LA-Trp at pH 11, the samples formed were colloidal, insoluble dispersions. The mean

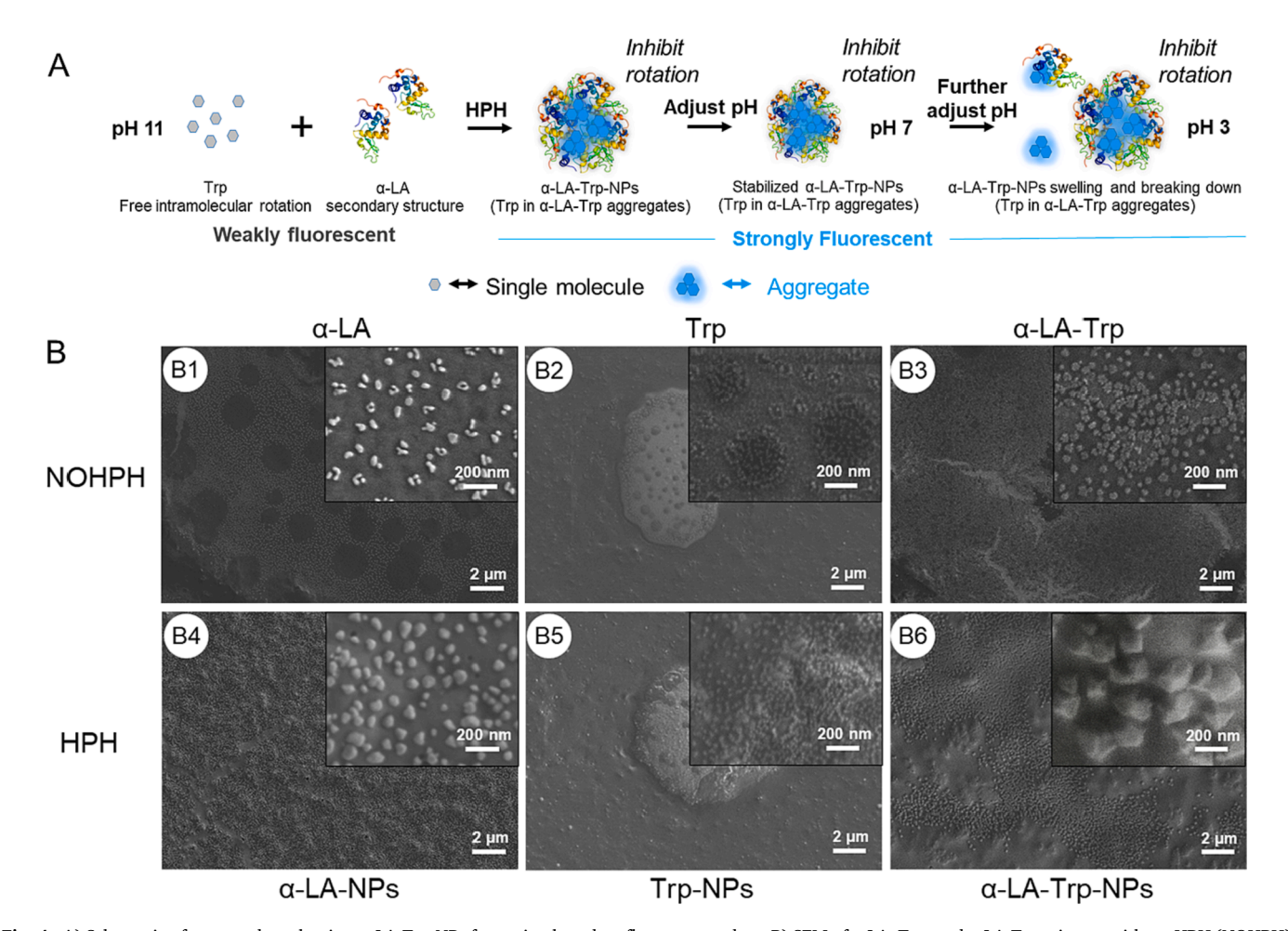


Fig. 4. A) Schematic of proposed mechanism  $\alpha$ -LA-Trp-NPs formation based on fluorescence data. B) SEM of  $\alpha$ -LA, Trp, and  $\alpha$ -LA-Trp mixture without HPH (NOHPH) (B1-3) as well as  $\alpha$ -LA-NPs, Trp-NPs, and  $\alpha$ -LA-Trp-NPs produced by HPH (B4-6).

particle size increased from  $\sim 2$  nm under NOHPH (Fig. 3B) to  $\sim 280$  nm with HPH (Fig. 3C and Table S2), suggesting the aggregation of  $\alpha$ -LA, Trp, and the  $\alpha$ -LA-Trp complex to form larger sized particles under high pressure, high shear, and cavitation. The NPs formed were maintained after shifting pH from 11 to 7 and from 11 to 3 (Fig. 3B and C). Therefore, we concluded that HPH plays an important role in the formation of the  $\alpha$ -LA-Trp-NPs and that while the NPs are robust under pH shifting, there is a small decrease in size.

#### 3.4. Potential mechanism of NPs formation by HPH and pH shifting

Weak fluorescence emission is observed for  $\alpha$ -LA-Trp mixtures at pH 11 without HPH because the protein and the Trp are in free molecular forms. However, when HPH is applied the emission intensity of the same samples prepared at pH 11 increases. The changes in fluorescence intensity varied under different HPH and pH shifting conditions. Therefore, we speculated that HPH increased  $\alpha$ -LA and Trp aggregation which triggered the turn on mechanism for the Trp chromophore for all samples. When the pH was adjusted from pH 11 to 7 or 11 to 3, the results remained consistent: NOHPH samples were weakly fluorescent and HPH samples showed higher fluorescence intensity. There are two reported explanations for this. First, exposure of internal tryptophan residues to the protein surface will result in a decrease of the fluorescence intensity due the solvent quenching. Buried tryptophan residue, however, will be less affected by the presence of the solvent and thus will show strong fluorescence (Stănciuc et al., 2012; Toptygin et al., 2002; Vivian & Callis, 2001). Second, the fluorescence of the Trp chromophore indicates that free Trp molecules are mostly nonfluorescent due to rapid nonradiative decay via twisted-intramolecular charge transfer (TICT) which is blocked when the molecules are locked in place by proteins, protein aggregates, and self-assemblies causing high fluorescence (Carayon et al., 2016; Liu, Wolstenholme, et al., 2018). Therefore, we propose that  $\alpha$ -LA-Trp-NPs formed by HPH have Trp molecules buried deeply within the protein structure as aggregates, which would reduce the impacts of solvent quenching and inhibit TICT, thus resulting in higher fluorescence (Fig. 4A). Prior to undergoing HPH at pH 11, unincorporated Trp molecules and Trp within the protein experienced active intramolecular rotation in an alkaline environment, leading to nonradiative relaxation of the excited molecules and resulting in weak fluorescence (Fig. 4A). However, upon HPH treatment and the subsequent formation of molecular aggregates of  $\alpha$ -LA and Trp, the intramolecular rotation becomes restricted, effectively blocking the nonradiative relaxation pathway. Consequently, the restriction of intramolecular rotation facilitated nonradiative decay leads to the strong fluorescence of the  $\alpha$ -LA-Trp-NPs.

The slight decrease observed in the fluorescence maximum emission intensity and wavelength of α-LA-Trp-NPs due to pH shifting from 11 to 7 may be due to differences in their molecule/aggregate structure. The particle size decreased after pH shifting from ~283 nm at pH 11 to  $\sim$ 243 nm at pH 7. This means that more of the Trp in the mixture could be exposed to the solvent and thus the fluorescence suffered from solvent induced quenching. Studies of pH-dependent disassembly and reassembly of proteins have proposed that at higher pH proteins unfold and disassemble; then when the pH is shifted to lower pH, they refold and reassemble at neutral pH (Tang, 2020; Tang et al., 2009). Therefore, we propose that as the pH shifts from 11 to 7, the α-LA-Trp-NPs contract and show smaller particle size and thus we observe a decrease in fluorescence intensity due to solvent quenching of Trp that is closer to the surface of the protein (Fig. 4A). When further shifted pH to 3, the  $\alpha$ -LA-Trp-NPs swell as the protein unfolds at pH 3 and the NPs partially break down, releasing small size particles and thereby the fluorescence intensity further decrease.

The SEM micrograph of NOHPH and HPH samples for  $\alpha$ -LA, Trp, and  $\alpha$ -LA-Trp-NPs as 1 mg mL $^{-1}$  dispersions illustrated the differences observed in the morphology of the samples (Fig. 4B). The NOHPH samples showed small size aggregates, while larger size aggregates were observed for HPH samples, further confirmed the aggregation of  $\alpha$ -LA

and Trp during HPH. The NOHPH sample of  $\alpha\text{-LA}$  exhibited globular particles with particle sizes around 40 nm (Fig. 4B1), versus the sample after HPH where the particle size was  $\sim\!80$  nm (Fig. 4C4). The particle size in the dry state was much smaller than the hydrodynamic particle size measured by DLS (Fig. 3) due to the dehydration of the particle and the different measurement techniques used. The relative size of the all the HPH samples to their corresponding NOHPH samples was consistently larger. The mixtures of  $\alpha\text{-LA}$  and Trp, however, showed different morphology than either that of  $\alpha\text{-LA}$  or Trp; the structures appeared more crystalline and had less globular shapes before and after HPH. The HPH sample of  $\alpha\text{-LA-Trp-NPs}$  showed homogenous polygonal particles with size of  $\sim\!180$  nm. These particles were very different both in morphology and size when compared to  $\alpha\text{-LA}$  and Trp. This is further evidence of the complex nanoparticles formation between  $\alpha\text{-LA}$  and Trp after HPH and is consistent with the results of Trp fluorescence.

The FT-IR of  $\alpha$ -LA and Trp mixture and their NPs formed at pH 11 via HPH and pH shifting revealed that their chemical composition remained unchanged throughout the HPH and pH shifting process (Fig. S2). Despite undergoing these treatments, the characteristic peaks and bands corresponding to the molecular vibrations of the components present in  $\alpha$ -LA-Trp-NPs remained consistent, indicating that the primary chemical structure of the NPs was not altered. This finding suggests that HPH and pH shifting had minimal impact on the overall chemical makeup of the  $\alpha$ -LA and Trp mixture, implying that the observed NPs formation and changes in their properties, such as particle size and stability, were likely attributed to variations in their physical arrangement and non-covalent interactions such as hydrophobic interaction, electrostatic interactions, and hydrogen bonds, rather than chemical transformations.

# 3.5. Effect of HPH and pH shifting on the thermal stability of $\alpha$ -LA-Trp-NPs

All HPH treated samples,  $\alpha$ -LA-NPs, Trp-NPs, and  $\alpha$ -LA-Trp-NPs were incubated at 63 °C for 30 min and a separate set of samples were incubated at 90 °C for 2 min to approximate food processing conditions, and their appearance, turbidity, particle size, and particle size distribution were used to evaluate thermal stability. When we compared the appearance of the colloidal dispersions of the HPH treated mixtures before and after thermal treatments, no changes were observed indicating good thermal stability (Fig. 5A). We speculate that the particles formed by HPH remained intact during heat processing and this was confirmed by the results of particle size measurements (Fig. 5B). The particle size distribution of the samples after heat treatments ranged from 70 nm to 3000 nm, which is greater than the particle size of  $\alpha$ -LA and Trp in their molecular form (<10 nm, Fig. 3B). This suggested the inter- or intramolecular associations induced by HPH are maintained upon heating.

The mean particle sizes (Z-average) of α-LA-Trp-NPs at pH 11 increased from  $\sim$ 283 nm to  $\sim$ 537 nm when heated at 63 °C for 30 min and from  $\sim$ 290 nm to  $\sim$ 520 nm when heated at 90  $^{\circ}$ C for 2 min. The PDI values of  $\alpha$ -LA-Trp-NPs did not change significantly (p > 0.05) upon heating at pH 11 (PDI < 0.2) indicating that the particles in the dispersion are uniform with narrow particle size distribution (Fig. 5B). The increase in particle size of α-LA-Trp-NPs at pH 11 after heat treatments was greater than those of  $\alpha$ -LA-NPs. For example, the particle size of  $\alpha$ -LA-Trp-NPs increased from  $\sim$ 283 to 537 nm upon heating at 63  $^{\circ}$ C, 30 min, while that of  $\alpha$ -LA-NPs increased from  $\sim$ 289 to  $\sim$ 445 nm. The growth of the particle size after heating was attributed to the swelling of the particles and the observed difference may be due to the presence of Trp in the NPs. When the protein is complexed with Trp, there are fewer protein-protein interactions during HPH at pH 11, as a result, the proteins have more freedom of motion, which promotes swelling of the α-LA-Trp-NPs upon heating.

The mean particle size of  $\alpha$ -LA-Trp-NPs which were pH shifted from pH 11 to pH 7 and incubated at pH 7 did not change greatly after incubation at either 63 °C for 30 min (243 to 258 nm) or at 90 °C for 2 min

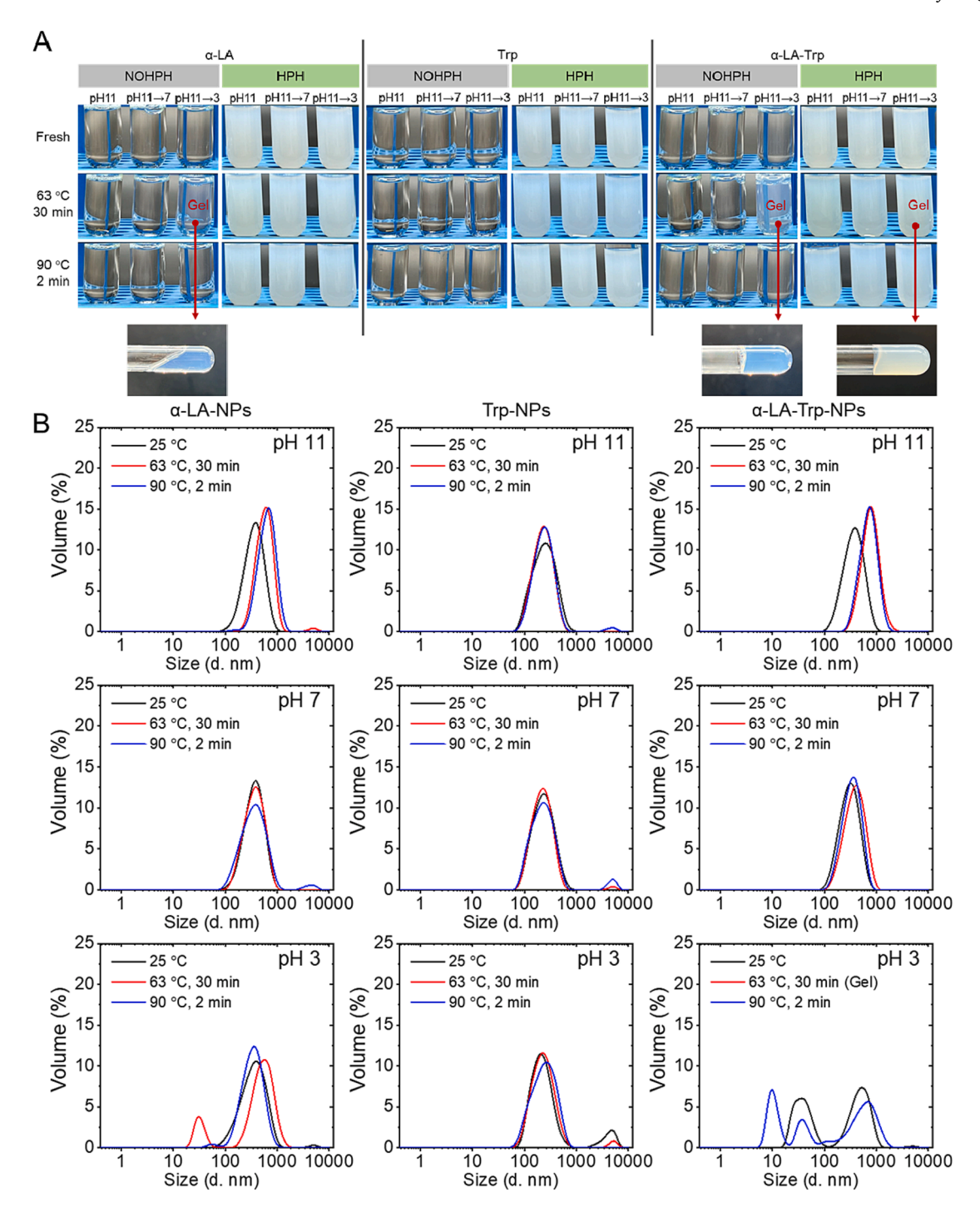


Fig. 5. A) Effect of thermal treatments on the colloidal stability of  $\alpha$ -LA, Trp, and  $\alpha$ -LA-Trp mixture. HPH (High pressure homogenization, samples with HPH treatment); NOHPH (control samples without HPH treatment); B) Particle thermal stability analysis of  $\alpha$ -LA-NPs, Trp-NPs, and  $\alpha$ -LA-Trp-NPs after HPH treatment. NPs were formed at  $\alpha$ -LA/Trp ratio of 5:1, 206.8 MPa, 40 min at pH 11 and those with pH shifting from 11 to 7 and 11 to 3.

(243 nm to 254 nm) (Fig. 5B and Table S3). We also observed that there was no significant change in the particle size and particle size distribution of  $\alpha$ -LA-NPs and  $\alpha$ -LA-Trp-NPs with pH shifting from 11 to 7 upon heating (Table S3 and Fig. 5B). This unique characteristic of  $\alpha$ -LA-NPs and  $\alpha$ -LA-Trp-NPs at pH 7 may be attributed to specific inter- or intramolecular associations of the protein, such as protein folding within the nanoparticles. These associations could include hydrophobic interactions, electrostatic interactions, or hydrogen bonds, which are likely formed during the pH shifting process. It is plausible that these interactions provide protection against swelling and thermal degradation during heating (Jiang et al., 2009, 2018; Tang, 2020). Previous

studies on the thermal stability of protein structures also reported that pH shifting could improve the thermal stability of protein (Jiang et al., 2009, 2010).

In comparison to  $\alpha$ -LA-NPs, the  $\alpha$ -LA-Trp-NPs were less thermally stable when the pH is shifted from pH 11 to pH 3 due to the presence of Trp. After thermal treatments at pH 3, both  $\alpha$ -LA-NPs and  $\alpha$ -LA-Trp-NPs exhibited noticeable swelling and partial breakdown to varying degrees. Specifically, the dispersion of  $\alpha$ -LA-NPs did not undergo great change after incubation at both 63 °C for 30 min and 90 °C for 2 min. By contrast, the dispersion of  $\alpha$ -LA-Trp-NPs showed a gel-like structure after incubation at 63 °C for 30 min (Fig. 5A). Both  $\alpha$ -LA-NPs and  $\alpha$ -LA-

Trp-NPs exhibited higher thermal stability when subjected to 90 °C for 2 min, and no gel formation occurred under these conditions. Overall, the thermal effects of samples incubated at pH 3 led to various unfavorable outcomes, such as an increase or decrease in particle size, the appearance of multi-peak particle size distribution, or the formation of a gellike structure (Fig. 5). These observations highlight the sensitivity of the protein containing NPs to the combined influence of low pH and elevated temperatures, which can result in structural alterations and

compromised stability.

The particle size of Trp-NPs did not change significantly upon heating at all pHs, which can be attributed to the presence of stronger intermolecular forces such as  $\pi$ - $\pi$  stacking between Trp molecules. These intermolecular interactions create a more stable structure that requires higher energy to overcome, limiting the extent of swelling during the heating process (Bhangu et al., 2020).

Overall, the thermal stability of the  $\alpha$  -LA-Trp-NPs at pH 11 and after

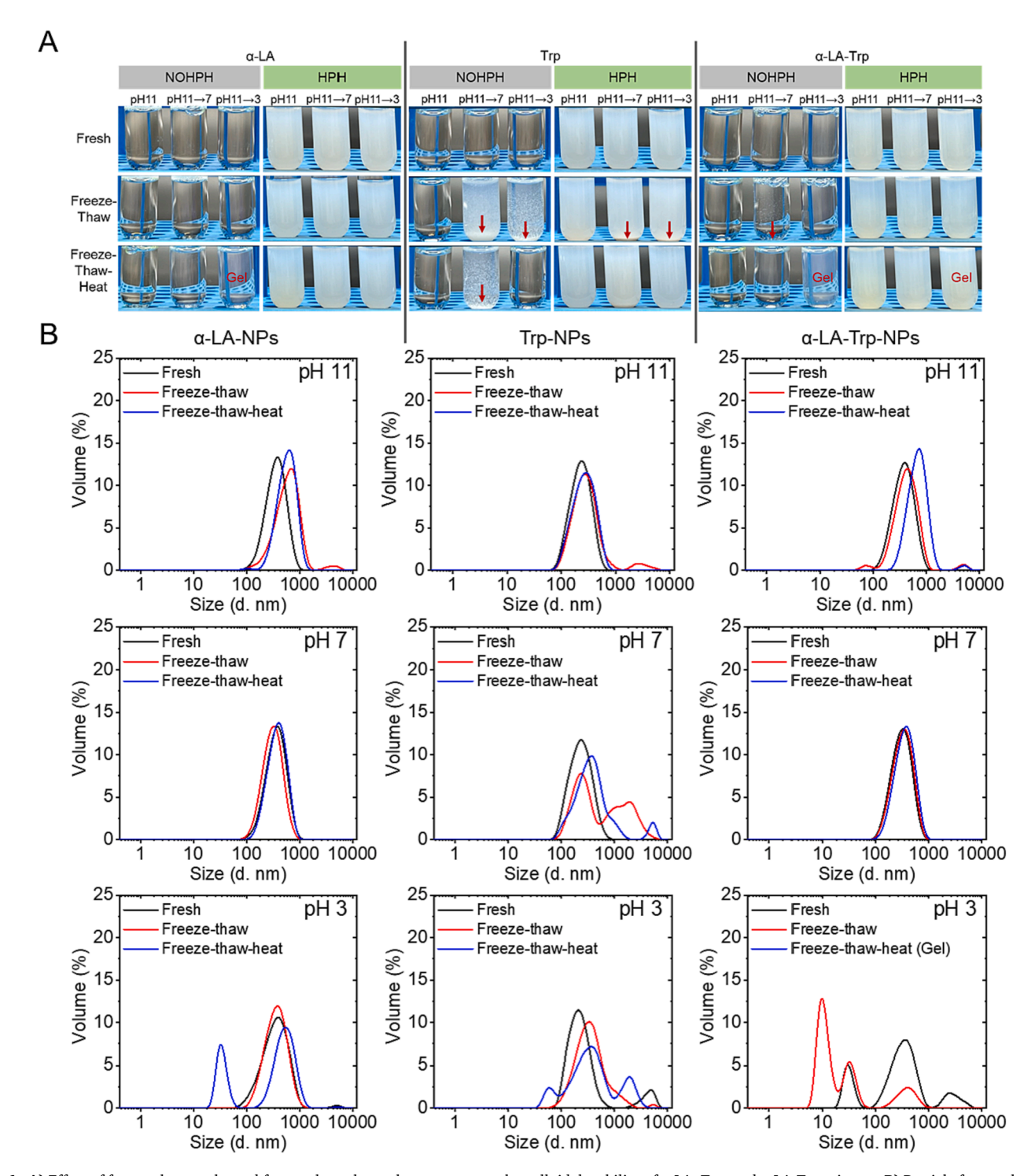


**Fig. 6. A)** Effect of freeze–thaw cycle, and freeze–thaw-thermal treatments on the colloidal stability of  $\alpha$ -LA, Trp, and  $\alpha$ -LA-Trp mixture. **B)** Particle freeze–thaw and freeze–thaw-thermal stability analysis of  $\alpha$ -LA-NPs, Trp-NPs, and  $\alpha$ -LA-Trp-NPs made through HPH treatment. HPH (High-pressure homogenization, samples with HPH treatment); NOHPH (control samples without HPH treatment); Insert arrow suggests the presence of sediments in the sample. NPs were formed at  $\alpha$ -LA/Trp ratio of 5:1, 206.8 MPa, 40 min at pH 11 and those with pH shifting from 11 to 7 and 11 to 3.

pH shifting from 11 to 7, is a useful property for beverage and nutritional product applications that involve Trp fortified ingredients in their formulations and that are exposed to high temperature treatments.

# 3.6. Effect of HPH and pH shifting on the freeze–thaw and freeze–thaw-thermal stability of $\alpha$ -LA-Trp-NPs at different pH

The physical stability of our NPs-based delivery systems during freeze–thaw and freeze–thaw-thermal cycles is important for products intended for use as a food ingredient. We subjected freshly prepared solutions of our  $\alpha\text{-LA-Trp-NPs},~\alpha\text{-LA-NPs}$  and Trp-NPs to freeze–thaw and freeze–thaw-thermal stability conditions designed to mimic or exceed food industry conditions. For the freeze–thaw cycle, the samples were subjected to extreme changes in storage temperature from - 20 °C to 25 °C and then for the freeze–thaw-thermal cycles the samples underwent an additional heat treatment at 63 °C for 30 min.

The particle size of the α-LA-NPs increased slightly after the freeze--thaw treatment at pH 11, and then grew again after the heat treatment (Fig. 6 and Table S3). The increase in particle size of proteins after a freeze-thaw has been reported, and it is generally attributed to protein aggregation caused by the growing ice crystals during freezing (Chen et al., 2022). The growth of the particle size at pH 11 after heating is consistent with the result for samples without freeze-thaw, where no observable differences observed in particle size and PDI values (Fig. 6 and Table S3). This may be due to the protein aggregation that occurred during freezing which was subsequently broken-down during heating allowing the NPs to increase in size due to swelling. Samples that were pH shifted from pH 11 to pH 7, however, exhibited no apparent change in the particle size of  $\alpha$ -LA-NPs after freeze-thaw treatment nor after the freeze-thaw-thermal cycles. This result indicated that the freeze-thaw cycle did not significantly impact the colloidal dispersion stability of  $\alpha$ -LA-NPs, and therefore, the particle stability of  $\alpha$ -LA-NPs was improved by pH shifting, which is consistent with the folded and more compact structure of the  $\alpha$ -LA being more robust.

Conversely, the Trp-NPs showed markedly different behaviors, exhibiting freeze—thaw stability at pH 11 with poor freeze—thaw stability at pH 7 (Fig. 6A). Sedimentation of particles was visually observed after freeze—thaw in Trp-NPs dispersions at pH 7 (Fig. 6A), which is consistent with increased turbidity (Table S3).

The particle size of  $\alpha$ -LA-Trp-NPs at pH 11 was not influenced significantly by the freeze–thaw cycle (Table S3 and Fig. 6B). After heat treatment at pH 11, the particle size increased slightly, but the size distribution remained narrow. The presence of Trp in the NPs increased the freeze–thaw stability of  $\alpha$ -LA-Trp-NPs at pH 11 by preventing the aggregation of protein during freezing. No visible aggregates observed in  $\alpha$ -LA-Trp-NPs dispersion with pH shifting from 11 to 7 after freeze–thaw and freeze–thaw-thermal treatment (Fig. 6A). With pH shifting from 11 to 7, the particle size of  $\alpha$ -LA-Trp-NPs was uniform and did not change significantly upon freeze–thaw and freeze–thaw-thermal treatment. This suggests that the presence of  $\alpha$ -LA increases the freeze–thaw and freeze–thaw-thermal stability of Trp through complex formation via the synergistic effects of HPH and pH shifting.

The  $\alpha$ -LA-Trp-NPs with pH shifting from 11 to 3 demonstrate reduced stability as they swelled and partially deteriorated during the pH shifting process from 11 to 3. This initial destabilization makes the nanoparticles more susceptible to further breakdown during the subsequent freeze—thaw cycle. The freeze—thaw process, involving the formation of ice crystals and temperature fluctuations, exacerbates the fragility of the nanoparticles, leading to additional structural disruptions and alterations in particle size and size distribution (Chen et al., 2022). Moreover, the reduced stability of  $\alpha$ -LA-Trp-NPs with pH shifting from 11 to 3 also manifests during the freeze—thaw-thermal treatment, where they tend to undergo gel formation (Fig. 6A). The combined effects of with pH shifting from 11 to 3 and elevated temperatures intensify the protein—protein interactions and altered the structural conformation of the nanoparticles, resulting in the formation of gel-like structures. These

observations are consistent with the thermal stability results, and in comparison to  $\alpha$ -LA-NPs, the  $\alpha$ -LA-Trp-NPs were less freeze—thaw-thermally stable with pH shifting from 11 to 3 due to the presence of Trp.

Based on the above findings,  $\alpha$ -LA-Trp-NPs formed using HPH and pH shifting to pH 7 are considered a promising shelf stable food formulation. The structural characteristics of  $\alpha$ -LA-Trp-NPs as influenced by freeze—thaw and freeze—thaw-thermal treatment would be further investigated in the future study.

#### 4. Conclusion

Trp rich NP ingredients were successfully fabricated from  $\alpha$ -LA and Trp using a combination of high-pressure homogenization (HPH) and pH-shifting. The α-LA-Trp-NPs particle size and particle size distribution could be controlled by changing the processing parameters, such as  $\alpha$ -LA to Trp ratios, the HPH pressure, and recirculation time. The optimum that provided the highest concentration of  $\alpha$ -LA to Trp mass ratio and smallest particle size were: HPH at 206.8 MPa for 40 min with a total concentration of 100 mg mL<sup>-1</sup> at an  $\alpha$ -LA to Trp ratio of 5:1 at pH 11 followed by pH shifting to pH 7. With this technique, a colloidal dispersion of  $\alpha$ -LA-Trp-NPs with a mean particle size of  $\sim$ 230 nm with a narrow particle size distribution (PDI < 0.3) was obtained. The formation of the α-LA-Trp-NPs followed a controlled HPH-induced aggregation mechanism; the Trp is incorporated into the soluble unfolded protein at pH 11; with HPH the α-LA-Trp-NPs become increasingly insoluble; and finally with pH shifting from 11 to 7 the  $\alpha$ -LA-Trp-NPs formed stable, small particles as the protein folds around and protects the Trp.

The  $\alpha\text{-LA-Trp-NPs}$  formed were homogenous polygonal particles. The thermal, freeze–thaw, and freeze–thaw-thermal stability of the  $\alpha\text{-LA-Trp-NPs}$  formed at pH 11 were improved by pH shifting from pH 11 to pH 7. Compared to NPs of Trp alone, the  $\alpha\text{-LA-Trp-NPs}$  showed better stability upon freeze–thaw cycle and freeze–thaw-thermal treatment. The  $\alpha\text{-LA-Trp-NPs}$  are also found to exhibit remarkable stability against thermal treatments at 63 °C, 30 min and 90 °C, 2 min as well as freeze–thaw-thermal treatment, which can be useful for applications in beverages and other liquid-type food and nutritional products.

### CRediT authorship contribution statement

Hongmin Dong: Conceptualization, Methodology, Validation, Formal analysis, Investigation, Data curation, Writing – original draft. Lixin Yang: Methodology, Validation, Investigation, Writing – review & editing. Younas Dadmohammadi: Conceptualization, Methodology, Project administration, Writing – review & editing. Peilong Li: Methodology, Investigation, Writing – review & editing. Tiantian Lin: Conceptualization, Methodology, Writing – review & editing. Yanhong He: Methodology, Writing – review & editing. Yufeng Zhou: Methodology, Writing – review & editing. Jieying Li: Methodology, Writing – review & editing. Gopinathan Meletharayil: Resources, Writing – review & editing. Alireza Abbaspourrad: Conceptualization, Methodology, Resources, Writing – review & editing, Supervision, Project administration, Funding acquisition.

### **Declaration of Competing Interest**

The authors declare that they have no known competing financial interests or personal relationships that could have appeared to influence the work reported in this paper.

# Data availability

Data will be made available on request.

#### Acknowledgments

This research was supported by the Dairy Management Inc. (Rosemont, IL). The researchers used the Cornell Center for Materials Research Shared Facilities which are supported through the NSF MRSEC program (DMR-1719875).

#### Appendix A. Supplementary data

Supplementary data to this article can be found online at  $\frac{\text{https:}}{\text{doi.}}$  org/10.1016/j.foodchem.2023.137371.

#### References

- Bhangu, S. K., Ashokkumar, M., & Cavalieri, F. (2020). Synthesis of bio-functional nanoparticles from sono-responsive amino acids using high frequency ultrasound. *Ultrasonics Sonochemistry*, 63, Article 104967. https://doi.org/10.1016/j. ultsonch.2020.104967
- Carayon, C., Ghodbane, A., Gibot, L., Dumur, R., Wang, J., Saffon, N., ... Fery-Forgues, S. (2016). Conjugates of benzoxazole and GFP chromophore with aggregation-induced enhanced emission: influence of the chain length on the formation of particles and on the dye uptake by living cells. Small, 12(47), 6602–6612. https://doi.org/10.1002/smll.201602799
- Chen, Y., Yi, X., Zhang, Z., Ding, B., Li, Z., & Luo, Y. (2022). High internal phase Pickering emulsions stabilized by tannic acid-ovalbumin complexes: Interfacial property and stability. Food Hydrocolloids, 125, Article 107332. https://doi.org/ 10.1016/j.foodhyd.2021.107332
- De, S. K., Maity, A., & Chakraborty, A. (2021). Underlying mechanisms for the modulation of self-assembly and the intrinsic fluorescent properties of amino acidfunctionalized gold nanoparticles. *Langmuir*, 37(16), 5022–5033. https://doi.org/ 10.1021/acs.langmuir.1c00431
- Di Pizio, A., & Nicoli, A. (2020). In silico molecular study of tryptophan bitterness. Molecules (Basel, Switzerland), 25(20). https://doi.org/10.3390/molecules25204623
- Friedman, M. (2018). Analysis, nutrition, and health benefits of tryptophan. *International Journal of Tryptophan Research*, 11, Article 1178646918802282. https://doi.org/10.1177/1178646918802282
- Jiang, J., Chen, J., & Xiong, Y. L. (2009). Structural and emulsifying properties of soy protein isolate subjected to acid and alkaline pH-shifting processes. *Journal of Agricultural and Food Chemistry*, 57(16), 7576–7583. https://doi.org/10.1021/ if901585n
- Jiang, J., Wang, Q., & Xiong, Y. L. (2018). A pH shift approach to the improvement of interfacial properties of plant seed proteins. Current Opinion in Food Science, 19, 50–56. https://doi.org/10.1016/j.cofs.2018.01.002
- Jiang, J., Xiong, Y. L., & Chen, J. (2010). PH shifting alters solubility characteristics and thermal stability of soy protein isolate and its globulin fractions in different pH, salt concentration, and temperature conditions. *Journal of Agricultural and Food Chemistry*, 58(13), 8035–8042. https://doi.org/10.1021/jf101045b
- Ley, J. P. (2008). Masking bitter taste by molecules. Chemosensory Perception, 1(1),  $58\text{--}77.\ https://doi.org/10.1007/s12078-008-9008-2$
- Liu, Y., Fan, Y., Gao, L., Zhang, Y., & Yi, J. (2018). Enhanced pH and thermal stability, solubility, and antioxidant activity of resveratrol by nanocomplexation with α-lactalbumin. Food & Function, 9(9), 4781–4790. https://doi.org/10.1039/C8F001172A
- Liu, Y., Wolstenholme, C. H., Carter, G. C., Liu, H., Hu, H., Grainger, L. S., ... Zhang, X. (2018). Modulation of fluorescent protein chromophores to detect protein aggregation with turn-on fluorescence. *Journal of the American Chemical Society*, 140 (24), 7381–7384. https://doi.org/10.1021/jacs.8b02176
- Ma, L., Li, A., Li, T., Li, M., Wang, X., Hussain, M. A., ... Hou, J. (2020). Structure and characterization of laccase-crosslinked α-lactalbumin: Impacts of high pressure homogenization pretreatment. *LWT*, 118, Article 108843. https://doi.org/10.1016/ j.lwt.2019.108843

- Mehrad, B., Ravanfar, R., Licker, J., Regenstein, J. M., & Abbaspourrad, A. (2018). Enhancing the physicochemical stability of β-carotene solid lipid nanoparticle (SLNP) using whey protein isolate. Food Research International, 105, 962–969. https://doi.org/10.1016/j.foodres.2017.12.036
- Roca, M., Althaus, R. L., & Molina, M. P. (2013). Thermodynamic analysis of the thermal stability of sulphonamides in milk using liquid chromatography tandem mass spectrometry detection. *Food Chemistry*, 136(2), 376–383. https://doi.org/10.1016/ i.foodchem.2012.08.055
- Rudolph, S., Riedel, E., & Henle, T. (2018). Studies on the interaction of the aromatic amino acids tryptophan, tyrosine and phenylalanine as well as tryptophancontaining dipeptides with cyclodextrins. European Food Research and Technology, 244(9). https://doi.org/10.1007/s00217-018-3065-9
- Saricaoglu, F. T., Gul, O., Tural, S., & Turhan, S. (2017). Potential application of high pressure homogenization (HPH) for improving functional and rheological properties of mechanically deboned chicken meat (MDCM) proteins. *Journal of Food Engineering*, 215, 161–171. https://doi.org/10.1016/j.jfoodeng.2017.07.029
- Stănciuc, N., Aprodu, I., Râpeanu, G., & Bahrim, G. (2012). Fluorescence spectroscopy and molecular modeling investigations on the thermally induced structural changes of bovine β-lactoglobulin. *Innovative Food Science and Emerging Technologies*, 15, 50–56. https://doi.org/10.1016/j.ifset.2012.03.001
- Tang, C.-H. (2020). Globular proteins as soft particles for stabilizing emulsions: Concepts and strategies. Food Hydrocolloids, 103, Article 105664. https://doi.org/10.1016/j. foodhyd.2020.105664
- Tang, C.-H., Wang, X.-Y., Yang, X.-Q., & Li, L. (2009). Formation of soluble aggregates from insoluble commercial soy protein isolate by means of ultrasonic treatment and their gelling properties. *Journal of Food Engineering*, 92(4), 432–437. https://doi.org/ 10.1016/j.ifoodeng.2008.12.017
- Toptygin, D., Savtchenko, R. S., Meadow, N. D., Roseman, S., & Brand, L. (2002). Effect of the solvent refractive index on the excited-state lifetime of a single tryptophan residue in a protein. *The Journal of Physical Chemistry. B*, 106(14), 3724–3734. https://doi.org/10.1021/jp0133889
- Vivian, J. T., & Callis, P. R. (2001). Mechanisms of tryptophan fluorescence shifts in proteins. *Biophysical Journal*, 80(5), 2093–2109. https://doi.org/10.1016/S0006-3495(01)76183-8
- Wei, G., Su, Z., Reynolds, N. P., Arosio, P., Hamley, I. W., Gazit, E., & Mezzenga, R. (2017). Self-assembling peptide and protein amyloids: From structure to tailored function in nanotechnology. Chemical Society Reviews, 46(15), 4661–4708. https://doi.org/10.1039/C6CS00542.1
- Wu, F., Shi, X., Zou, H., Zhang, T., Dong, X., Zhu, R., & Yu, C. (2019). Effects of high-pressure homogenization on physicochemical, rheological and emulsifying properties of myofibrillar protein. *Journal of Food Engineering*, 263, 272–279. https://doi.org/10.1016/j.ifoodeng.2019.07.009
- Zhang, A., Wang, L., Song, T., Yu, H., Wang, X., & Zhao, X. (2022). Effects of high-pressure homogenization on the structural and emulsifying properties of a vegetable protein: Cyperus esculentus L. LWT, 153, Article 112542. https://doi.org/10.1016/j.lwt.2021.112542
- Zhang, Z., Li, Y., Lee, M. C., Ravanfar, R., Padilla-Zakour, O. I., & Abbaspourrad, A. (2020). The impact of high-pressure processing on the structure and sensory properties of egg white-whey protein mixture at acidic conditions. Food and Bioprocess Technology, 13(2), 379–389. https://doi.org/10.1007/s11947-019-02397-6
- Zhu, Y., Sun, X., Ding, J., Fan, F., Li, P., Xia, J., ... Fang, Y. (2021). Physicochemical and functional properties of a novel xanthan gum-lysozyme nanoparticle material prepared by high pressure homogenization. *LWT*, 143, Article 111136. https://doi. org/10.1016/j.lwt.2021.111136
- Toprakcioglu, Z., Challa, P., Xu, C., & Knowles, T. P. J. (2019). Label-free analysis of protein aggregation and phase behavior. ACS Nano, 13(12), 13940–13948. https://doi.org/10.1021/acsnano.9b05552
- Yu, Y., Guan, Y., Liu, J., Hedi, W., Yu, Y., & Zhang, T. (2021). Molecular structural modification of egg white protein by pH-shifting for improving emulsifying capacity and stability. Food Hydrocolloids, 121, Article 107071. https://doi.org/10.1016/j. foodbyd/2021.07071
- Zhu, X.-F., Zheng, J., Liu, F., Qiu, C.-Y., Lin, W.-F., & Tang, C.-H. (2017). The influence of ionic strength on the characteristics of heat-induced soy protein aggregate nanoparticles and the freeze–thaw stability of the resultant Pickering emulsions. Food & Function, 8(8), 2974–2981. https://doi.org/10.1039/C7F000616K